

Scottish Roads Research Board

**Scottish Trunk Road Fragility
to Extreme Precipitation**

Euan Macdonald,

Dr Enrico Tubaldi, Dr Neil Ferguson, Prof Edoardo Patelli

22/02/2024

Executive Summary

This report contains analysis of the fragility of the Scottish trunk road network to disruption from precipitation events. It begins with an explanation of the requirement for this type of analysis and the gap in the knowledge base that this report fills. Secondly there is a breakdown of the core concepts utilised in the report in order to build the fragility curves and consider the uncertainties at all stages in the process. Thirdly there is an inspection of the Transport Scotland IRIS database, SEPA point rainfall data and NIMROD radar precipitation estimates. Next, there is the analysis and presentation of the fragility curves for the disruption events. The report concludes with a discussion and a reflection on future works and improvements to the process.

Contents

Executive Summary	1
Contents	2
List of Figures	4
List of Tables	5
2. Database and Concept Review	9
2.1. Trunk Road Network and IRIS Database	9
2.2 Rainfall Interpolation	10
2.3. Fragility	11
3. Methodology	12
3.1. Event Identification	12
3.2. Kriging Data Sources	13
3.2.1. SEPA Data Quality	14
3.2.2. NIMROD Data Quality	15
3.3. Kriging Comparison	18
3.5. Fragility	21
4. Results	25
4.1. 1 Hour (Peak)	26
4.2. 3 Hour Cumulative	27
4.3. 6 Hour Cumulative	28
4.4. 12 Hour Cumulative	29
4.5. 24 Hour Cumulative	30
5. Conclusion and Discussions	31
Appendix	33
A.1.1 Expected Value and Semivariance	35
A.1.2. Simple Kriging	37
A.1.3. Ordinary Kriging	37
A.1.4. Universal Kriging	38
A.1.5. Kriging with External Drift	39
A.1.6. Regression Kriging	39

A.2. Fragility	41
A.3. Monte Carlo Method	43

List of Figures

Figure 1: Map of Scottish trunk road network.....	9
Figure 2: Location of events recorded as disruption caused in IRIS database and considered in this report.....	13
Figure 3: Location of SEPA weather stations.....	14
Figure 4: Correlation between hourly SEPA rainfall station observations and radar hourly rainfall estimates for the same location, against distance from the nearest radar station.....	16
Figure 5: NIMROD 1km radar for Scotland at 01/01/2015 averaged between 00:00 and 00:55.....	17
Figure 6: Example empirical fragility curve.....	23
Figure 7: Example distribution fit to dummy empirical conditional probability values.....	24
Figure 8: Example probability box for dummy distribution fits.....	24
Figure 9: Histogram of mean and lower and upper 95% confidence bounds for peak predictions associated with the 506 disruption events (left). Empirical Disruption/Conditional Probability Curve for Peak Rainfall (right).....	26
Figure 10: Cumulative distributions fitted to empirical conditional probability values for peak rainfall including UK maximum point (left). Probability box formed by the maximum and minimum values of all fitted distributions.....	26
Figure 11: Histogram of mean and lower and upper 95% confidence bounds for 3 hour cumulative predictions associated with the 506 disruption events (left). Empirical Disruption/Conditional Probability Curve for 3 hour cumulative rainfall (right).....	27
Figure 12: Cumulative distributions fitted to empirical conditional probability values for 3 hour cumulative rainfall including UK maximum point (left). Probability box formed by the maximum and minimum values of all fitted distributions.....	27
Figure 13: Histogram of mean and lower and upper 95% confidence bounds for 6 hour cumulative predictions associated with the 506 disruption events (left). Empirical Disruption/Conditional Probability Curve for 6 hour cumulative rainfall (right).....	28
Figure 14: Cumulative distributions fitted to empirical conditional probability values for 6 hour cumulative rainfall including UK maximum point (left). Probability box formed by the maximum and minimum values of all fitted distributions.....	28
Figure 15: Histogram of mean and lower and upper 95% confidence bounds for 12 hour cumulative predictions associated with the 506 disruption events (left). Empirical Disruption/Conditional Probability Curve for 12 hour cumulative rainfall (right).....	29
Figure 16: Cumulative distributions fitted to empirical conditional probability values for 12 hour cumulative rainfall including UK maximum point (left). Probability box formed by the maximum and minimum values of all fitted distributions.....	29
Figure 17: Histogram of mean and lower and upper 95% confidence bounds for 24 hour cumulative predictions associated with the 506 disruption events (left). Empirical Disruption/Conditional Probability Curve for 24 hour cumulative rainfall (right).....	30
Figure 18: Cumulative distributions fitted to empirical conditional probability values for 24 hour cumulative rainfall including UK maximum point (left). Probability box formed by the maximum and minimum values of all fitted distributions.....	30
Figure 19: variogram diagram (aspex 2019).....	36
Figure 20: Conditional probabilities for arbitrary intensity measure with regularly spaced intensities showing upper and lower limit of $\pm 20\%$	42

List of Tables

Table 1: Breakdown of flood related events in the IRIS database.	13
Table 3: Data mask SEPA rainfall stations for the period 01/01/2015 – 31/12/2021.	15
Table 4: Data Quality Check of Unchecked Values	15
At each point in the grid the product uses the highest quality and resolution data available and as such the quality of the composite radar product is dependent on both the quality and resolution of the source data. This in turn is dependent on distance from the nearest radar site (Stone, Harrison and Standing 2008). For Scotland these are radar stations are recorded in Table 5.	15
Table 5: Name and location of NIMROD radar stations in Scotland.	15
Table 4: Number of NIMROD 1km 5 minute resolution files present within each hour time step between 00:00 01/01/2015 and 23:55 31/12/2021. Total counts for each file number across the full timespan are recorded along with the percentage of the total number of hours observed across the full timespan.	17
Table 6: Name and proximity information to nearest rain gauge station.	18
Table 7: Kriging prediction metric results for all test point rainfall locations for 2021.	20
Table 8: Met Office UK rainfall records.	23

1. Introduction

Floods are a major cause of disruption to the transport sector, leading to significant direct and indirect losses. The extreme weather events occurring in recent years have resulted in considerable damages and prolonged disruptions to UK's transport networks. For example, widespread transport disruption occurred due to a succession of winter storms in 2013/14 and 2015/15 (Department For Transport, 2014) (BBC, 2016) and also more recently due to Storm Agnes and Babet. Flood risk in Scotland is expected to increase in the future because of climate change. According to the climate report by Adaption Scotland, as a result of climate change, Scotland will experience warmer, wetter winters, with more intense rainfall events (Adaption Scotland 2021). By 2050, under a low emissions scenario, average winters are projected to be around 8% wetter and 1 degree warmer. By 2080, under a high emissions scenario average winters are projected to be around 19% wetter and 2.7 degrees warmer. According to the Centre of Ecology and Hydrology (CEH) report (Kay & Crooks, 2011), a potential increase in regional flood peak for different emission scenarios for the 2080 time horizon can also be expected. The average increase in peak flow for the ten main river basins in Scotland has been estimated as 7-20% for low emission, 10-24% for medium emission, and 13-31% for high emission scenarios (Kay & Crooks, 2011).

Flooding can occur when moderate precipitation accumulates over several days, or when intense precipitation falls over a short period of time. It can also happen when ocean waves come on shore, when snow melts quickly, or when dams or levees break. The risk of disruption (R_D) associated with a hazardous event such as an extreme weather or a flood event can be expressed as the product of the probability of the hazard occurrence $P(H)$, the probability of disruption given the hazard $P(D|H)$ (denoted as “fragility” or “vulnerability”), and the consequences of disruption (C_D):

$$\text{Equation 1} \quad R_D = P(H) \times P(D|H) \times C_D$$

The hazard element of precipitation has been researched extensively with common practise to deploy depth-duration-frequency (DDF) or intensity-duration-frequency (IDF) curves. A DDF curve shows the expected height of rainfall for a given duration and frequency (Vesuviano 2022). The duration refers to the length of time that the rainfall event lasts, while the frequency refers to the probability of the rainfall event occurring in a given year. The intensity is the amount of rainfall that falls during the event, typically measured in millimetres per hour. IDF curves are useful for a variety of applications, including designing drainage systems and flood control measures. DDF and IDF curves are available or can be easily derived for any area in Scotland. Flood hazards can also be estimated, but this often requires the development of hydraulic models to transform the information on the precipitation into hydraulic parameters such as e.g. flood height and velocity.

Flooding can affect infrastructure in various ways, including physical damage to roads, bridges, and buildings, as well as disruptions to transportation services and as such it is very difficult to quantify the overall costs. A significant effort was made by the European Commission through the development of global flood depth-damage functions for many typologies of infrastructure assets (Huizinga, De Moel and Szewczyk 2017). The study concluded that between 4-18% of flood infrastructure damage was attributed to roads with urban areas being more affected than rural areas. In addition to direct physical damage, flooding often leads to indirect costs, such as business interruptions, loss of productivity, and increased transportation costs. These indirect costs are often more challenging to measure and quantify compared to direct physical damages. Analysis of these have been specifically carried out in a study focused on the vulnerability of roads in Scotland (Winter, et al. 2016). Quite surprisingly, there is a general lack of models for describing the fragility (or vulnerability) of roads.

Fragility analysis is an important tool for analysing the susceptibility of a system or structure to failure or damage under different conditions. In disaster models, fragility curves are frequently employed to establish the likelihood of surpassing a specific damage level based on the intensity of the hazard that triggers the disaster. Fragility curves play a crucial role in evaluating and mitigating the risk of road damage caused by flooding, offering valuable insights for infrastructure planning, design, and emergency response strategies. These curves can be broadly classified into three main categories, depending on the approach employed for deriving them: empirical, numerical, expert judgment, or combinations thereof.

Empirical fragility curves derive from observed data from historical events or experiments, making them data-driven and potentially reflective of real-world performance. However, this method requires a substantial amount of reliable, quality-assured data. In instances where this data is incomplete or unavailable, numerical methods can fill data gaps and model complex systems and interactions. Though, they are highly sensitive to model assumptions and demand a detailed understanding of physical processes and sophisticated computational tools, making them resource-intensive. A comprehensive comparison of empirical and numeric flood fragility and vulnerability methods is given by Galasso et al., (Galasso, Pregnolato and Parisi 2021).

By comparison, expert judgment offers a swift estimate in resource-limited scenarios and can integrate holistic knowledge. However, it heavily relies on the individual's expertise, making results susceptible to personal biases and lacking precision in quantifying damage states compared to the other two methods. An example of cross disciplinary expert judgement applied to multiple hazard transport fragility for roads subjected to debris flow is given in (Argyroudis, et al. 2019).

An empirical flood depth/disruption curve for road flooding was developed by Pregnolato et al. by fitting a relationship between the depth of standing water and vehicle speed (Pregnolato, et al. 2017).

This relationship was fit to data points that were a combination on of experimental study, road safety literature and from expert opinion. This relationship was then incorporating this into existing transport models to produce better estimates of flood induced delays.

In general, it is very difficult to gather information on the type of flooding and also on the intensity of the flooding event that has caused a disruption to a road. Thus, this study, in contrast to other studies in the literature, aims to establish fragility curves using parameters related to the precipitation as an intensity measure, without the ambition of classifying the flood hazard typology (i.e., pluvial, fluvial, or coastal).

Without fragility analysis, the quantification of the effective network risk is limited, increasing the likelihood that responsible authorities will make sub-optimal decisions on improvements to network development, robustness and resilience. Adapting and maintaining transport systems to remain resilient to the effects of climate change is part of the national transport strategy. The proposed fragility curves will provide a vital quantitative tool for network risk analysis and will aid in identifying parts of the network that are failing at a greater frequency than their design specifications. Additionally, the expected disruption to the road network for different emissions scenarios can be calculated using these fragility curves. This tool can also inform decisions regarding the management of network demand during extreme rainfall events. Effective management of network demand is a stipulation of the climate change act designed to help meet net-zero targets.

The rest of the report is organised as follows: Section 2 contains a review of the concepts used throughout the report, including a description of the trunk road network and Iris database, rainfall interpolation techniques and fragility analysis. Section 3 outlines the methodology that draws from these concepts. Section 4 presents the results of the analysis and section 5, the conclusions and recommendations for future work.

2. Database and Concept Review

This section provides the theory of the core concepts applied throughout this study. For readability, the order in which the information appears in the review is the same as the order in which the objectives are met in the methodology.

2.1. Trunk Road Network and IRIS Database

The Scottish trunk road network is a system of major roads in Scotland that are managed by Transport Scotland. The trunk road network includes some of the most important and busiest roads in Scotland, such as motorways, dual carriageways, and major single carriageway roads. These roads provide key connections between towns and cities, as well as access to ports, airports, and other important destinations. The Scottish trunk road network consists of over 3,500 miles of road and is Scottish Ministers' single biggest asset (Transport Scotland, The Trunk Road Network, Overview 2014). It has a gross asset value of over £20.8 billion and represents 6% of the total Scottish road network. It carries 35% of all traffic and 60% of heavy goods vehicles.

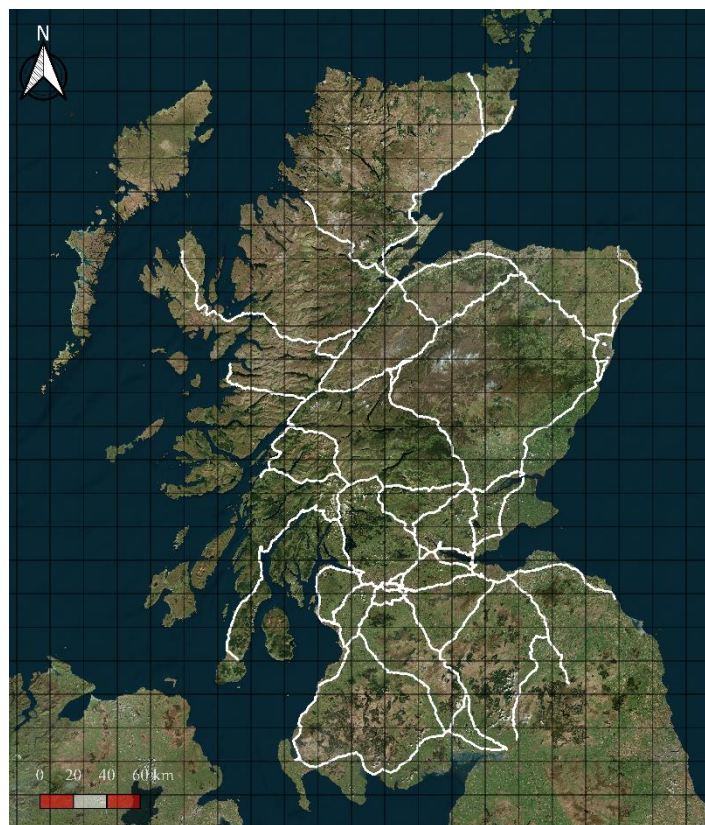


Figure 1: Map of Scottish trunk road network.

Transport Scotland has developed an asset management systems to gather information on trunk road assets and aid decision making. Collaborative efforts with the Welsh Government led to the procurement of a single contract for an Integrated Road Information System (IRIS) in 2012. IRIS is a fully integrated Geographical Information System (GIS) map-based asset management system that links

data on conditions, inventory, accidents, structures, drainage and maintenance. Transport Scotland currently uses IRIS functions along with other core systems to manage and maintain the trunk road network (Transport Scotland, Asset Management Systems and Data 2014).

As of August 2022, there are two companies that maintain the trunk road network in four regions of Scotland, known as the Operating Companies (OCs):

- BEAR Scotland - responsible for the South East and North West units
- Amey - responsible for the North East and South West units

Each OC is responsible for maintaining and improving the trunk roads in its area, including routine maintenance, winter maintenance, emergency response, and major projects (Transport Scotland, The Trunk Road Network, Operating Companies 2014). They work closely with Transport Scotland to ensure that the trunk road network is safe, efficient, and well-maintained. In the event of a road failure and the resulting call out of the operating company, the call out is logged in the IRIS Management of Incidents system (Transport Scotland, Asset Management Systems and Data 2014). It is worth highlighting that the true number of incidents that occur on the trunk road network is likely to be higher than is recorded in the IRIS database since the database only contains the events that are responded to by the operating companies. A further consideration is that the likelihood of attending an incident is unlikely to be uniform across all incident magnitudes as operating companies will prioritise the most severe events and so the probability that these will be represented in the IRIS database is higher. The variation in attendance probability with incident severity is not known.

2.2 Rainfall Interpolation

Interpolation methods are important techniques that allow for the estimation of values of a variable at points where it is not directly measured or observed. Many of the events that are reported in the IRIS database are not in close proximity to a weather station, hence the value of the rainfall must be estimated using an interpolation technique. Interpolation methods can be used to create continuous surfaces or maps of a variable, which can be easier to visualise and analyse than discrete data points. This can help to identify patterns and trends in the data, and to better understand the relationships between different variables. The most commonly applied interpolation methods are:

- *Natural Neighbour Interpolation*: the study area is divided into a network of Thiessen triangles and the unknown location value is estimated by averaging the values of the nearest observed points weighted by the area of their corresponding triangles.
- *Inverse Distance Weighting (IDW)*: the unknown location value is estimated as the weighted average of the values at nearby locations, with the weights decreasing as the distance from the target location increases.

- *Kriging*: the unknown location value is estimated based on a model of the spatial autocorrelation of the variable being interpolated, and the observations at nearby locations. Kriging is a popular method because it provides estimates of the interpolation error.

Multiple authors have investigated the comparison between basic mathematical interpolation methods such as Thiessen polygons and IDW and geostatistical interpolation methods such as Kriging, and the conclusion is that for low-density networks of rain gauges, Kriging outperforms the alternatives for daily, monthly and annual rainfall (Goovaerts 2000), (Mair 2011). Different types of kriging are compared in this study with the best performing selected to simulate the rainfall timeseries at the unknown locations.

Kriging, also known as Gaussian process regression, represents a full family of geostatistical interpolation techniques (Bhattacharjee 2019). They are used to predict the values of a random field at unobserved locations based on observations of the field at nearby locations. The method assumes that the random field being modelled is a realisation of a spatially continuous stochastic process, and the relationships between the values of the random field at different locations are described by a covariance function or semivariogram (Bhattacharjee 2019). The semivariogram is a plot of the variance of the difference between pairs of points as a function of the distance between them. The semivariogram provides information about the spatial structure of the variable being studied, such as its range and the degree of spatial dependence. This study considers four different types of kriging: ordinary, universal, external drift and regression. An explanation of each along with the equations that describe the processes are provided in the Appendix A.1.

2.3. Fragility

The fragility is a concept used in reliability engineering and risk analysis to assess the likelihood of a failure event given certain conditions or circumstances. It provides a measure of the probability that a system or component will fail, given that specific conditions or factors are present.

The process for developing a fragility curve for assessing the vulnerability of a critical road link to rainfall-induced failures, involves analysing the statistical relationship between rainfall intensity and the performance of the asset (whether it fails or not). Rainfall intensity is categorised into bins, and the conditional probability of failure for each bin is calculated by dividing the number of failures in that bin by the total number of rainfall events. The approach focuses on critical road sections that have experienced disruptions during a specified period.

To address uncertainty in rainfall intensity prediction using Kriging interpolation, a Monte Carlo analysis is incorporated. Kriging results in an uncertain prediction of rainfall intensity at unmonitored locations, with uncertainty described by a Gaussian distribution. The Monte Carlo technique involves

simulating numerous scenarios by drawing random values from input probability distributions, generated from the process variance of each Kriging model. This statistical analysis provides a distribution of results, allowing for the estimation of the probability of different outcomes and the overall risk associated with the system, instead of providing a single deterministic value. The complete process details are provided in Appendices A.2 and A.3.

3. Methodology

The objective of this study is to investigate the likelihood of experiencing a disruption in the road network due to extreme precipitation events, and to develop an empirical damage model for relating precipitation intensity to the probability of disruption. To this end, disruption events in the IRIS database are considered to assess the probability of failure for a given level of rainfall intensity. An event is considered a disruption event if it is classed as such in the IRIS database. For these events there is no knowledge of the rainfall intensity at the location site that is associated with the disruption and, so it is necessary to obtain an estimate of precipitation. A common geographical interpolation tool, regression kriging, is deployed, coupling point rainfall data from SEPA weather stations (SEPA n.d.), 1km radar data from NIMROD radar system (Met Office 2003), and location and altitude data (googleapis n.d.).

The fragility curve were constructed by first identifying road closure events from Transport Scotland’s IRIS database. A rainfall time series spanning the first to last disruption entry in the IRIS database was then estimated at each event location. The probability of a given rainfall intensity causing a road closure was calculated by dividing the number of events that a given rainfall intensity caused road closures at an affected location by the total number of times this intensity is observed at any affected location. Monte Carlo analysis was performed on the predicted precipitation values using the mean and the variance of the Kriging process to calculate the mean prediction and a confidence interval.

3.1. Event Identification

Table 1 provides the breakdown of the flood related events at the time of analysis spanning the period January 2015 to December 2021. The location of the 506 disruption events is shown in Figure 2.

Stage	Data Points
Iris Database	4898
Events that caused Disruption	569
Events that caused Disruption in window 01-01-2015 to 01-01-2021	506

Events that caused Disruption on A-Class sections (01-01-2015 to 01-01-2021) 393

Events that caused Disruption on M-Class sections (01-01-2015 to 01-01-2021) 113

Table 1: Breakdown of flood related events in the IRIS database.

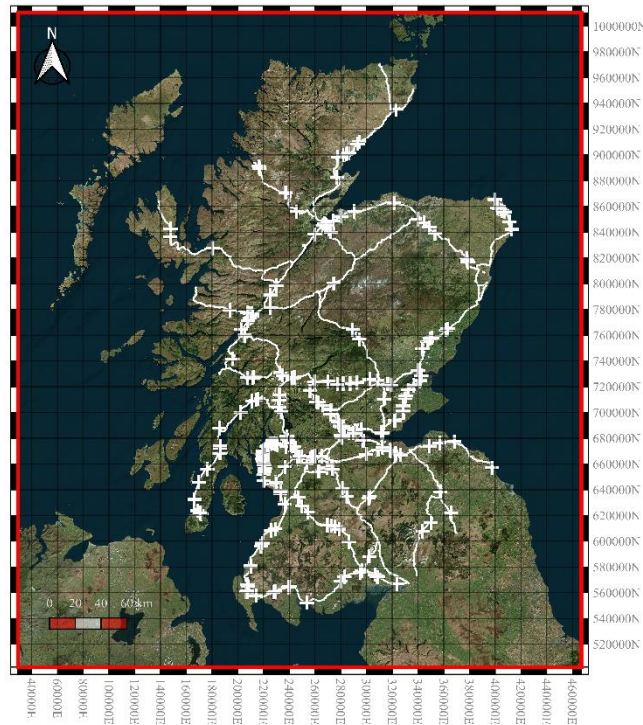


Figure 2: Location of events recorded as disruption caused in IRIS database and considered in this report.

3.2. Kriging Data Sources

For each of the 506 events recorded in Table 1, a time series of hourly rainfall was estimated spanning the period January 2015 to December 2021. In order to do this, different kriging methodologies were considered using combinations of the following inputs:

- OS Easting Northing
- Altitude
- SEPA rain station hourly rainfall
- NIMROD 1km radar

The OS Easting and Northing of the SEPA and radar rainfall data were stated with each dataset. The altitude variables were obtained by using the Google Elevation API. Figure 3 shows the location of the SEPA weather stations on a Map of Scotland.

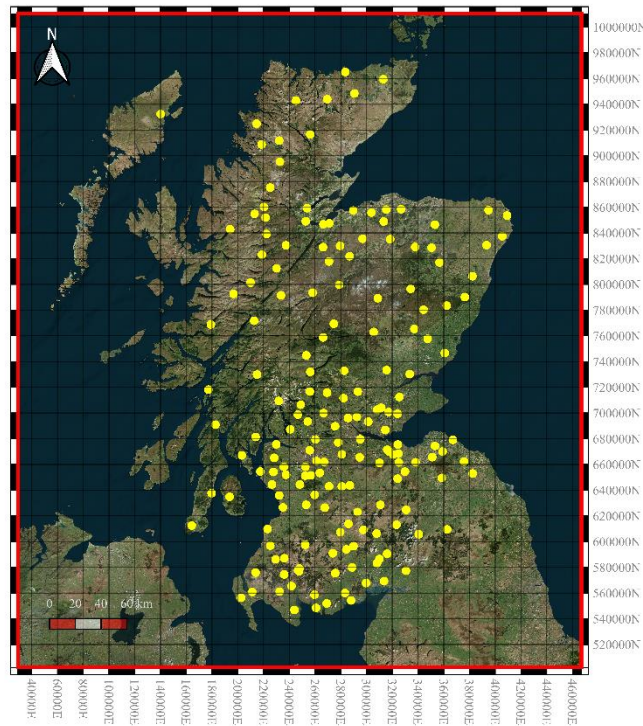


Figure 3: Location of SEPA weather stations.

3.2.1. SEPA Data Quality

Each SEPA timeseries was cropped to fit the time window 01/01/2015 to 31/12/2021. Accompanying the data was a quality code for each value. Bad values were removed from the analysis, and good values accepted. The remainder of the unchecked rainfall values were evaluated through a simple process of comparison with concurrent radar estimations for an encompassing area. Thereafter, a 5km box was drawn around each station location and the maximum and minimum radar value across that area were recorded along with the radar measurement at each location. Any unchecked point radar values that fell out with the radar range for the 5km box were indexed. Next, errors between the radar measurements and the station observations were calculated for checked rain gauge measurements. Any unchecked value that fell outside the checked error margin for the given intensity at that location was considered anomalous. Any station reading that was out with the radar range for the surrounding 5km and was flagged as an anomaly was considered suspicious and removed from the dataset. For timesteps that did not have a corresponding radar measurement, the values were checked against the nearest rain gauge stations to evaluate if the measurement was reasonable. The procedure was composed to ensure that observations would only be removed if there was compelling evidence to do so. The numbers of values flagged by SEPA are recorded in Table 2. The number of values flagged by the data quality procedure outlined above are recorded in Table 3.

	Count	% of total
Checked = 0	9,702,084	53.05
Unchecked = 1	7,966,444	43.56
Suspect = 2	619,136	3.39
Total	18,287,664	100

Table 2: Data mask SEPA rainfall stations for the period 01/01/2015 – 31/12/2021.

Treatment of Unchecked Sepa Values		
	Count	% of total
Not Suspect	7,952,281	99.82
Suspect	14,163	0.18
Total	7,966,444	100

Table 3: Data Quality Check of Unchecked Values

3.2.2. NIMROD Data Quality

The 1km NIMROD product is a UK wide composite of quality controlled and corrected surface precipitation values from the UK's network of C-band radars. Values are evaluated at 5 minute resolution on a Cartesian National Grid. The data has undergone extensive processing to correct for various sources of radar error such as noise, attenuation and range (Stone, Harrison and Standing 2008). The 1km gridded composite C-Band radar images of precipitation are calibrated with rain gauges. For full details see the NIMROD Radar Processing document (Harrison, Driscoll and Kitchen 1998).

At each point in the grid the product uses the highest quality and resolution data available and as such the quality of the composite radar product is dependent on both the quality and resolution of the source data. This in turn is dependent on distance from the nearest radar site (Stone, Harrison and Standing 2008). For Scotland these are radar stations are recorded in Table 4.

Name	Latitude	Longitude	Area
Munduff Hill	56°12'53"N	003°18'38"W	Fife
Hill of Dudwick	57°25'51"N	002°02'10"W	Aberdeenshire
Holehead	56°01'06"N	004°13'08"W	Stirling
Corse Hill	55°41'28"N	004°13'53"W	Strathclyde
Drium-a-Starraig	58°12'40"N	006°10'59"W	Isle of Lewis

Table 5: Name and location of NIMROD radar stations in Scotland.

The decrease of gridded radar data quality decreasing with distance is demonstrated here in Figure 4. The correlation between the SEPA hourly rainfall observations and NIMROD radar estimates

significantly decreases as the distance from the location to the nearest radar station increases. This is not a surprising result, and it follows that the value of radar information as a correlated variable for the external variable kriging methods is location dependent.

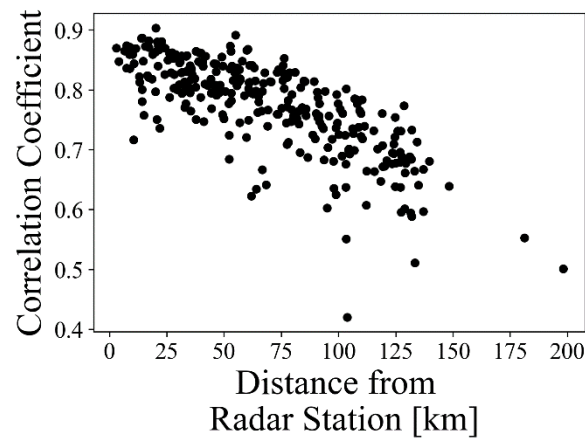


Figure 4: Correlation between hourly SEPA rainfall station observations and radar hourly rainfall estimates for the same location, against distance from the nearest radar station.

NIMROD 1km data was downloaded from CEDA (Met Office 2003) for the years 2015 to 2021. Files were cropped to the area of Scotland and hour average rainfall maps averaged from all available 5 minute resolution files for any given hour. To turn rainfall rates into mm/hr, NIMROD rates were divided by 32 to adjust values from the NIMROD system data saving standard which were integer precipitation rates in units of (mm/hr)*32. Figure 5 shows an example rainfall map from NIMROD for the 01/01/2015 averaged across the period 00:00 to 00:55. Table 6 shows the number of 5 minute NIMROD files present within each hour of the analysis.

File Count	Year							total	Total [%]
	2015	2016	2017	2018	2019	2020	2021		
0	295	121	131	129	148	283	20	1127	1.837
1	8	10	19	3	4	2	1	47	0.076
2	4	4	3	0	1	2	1	15	0.024
3	7	7	5	5	3	2	0	29	0.047
4	1	6	5	0	1	1	2	16	0.026
5	8	2	2	2	4	3	4	25	0.041
6	3	4	9	3	0	3	2	24	0.039
7	5	4	5	1	0	1	3	19	0.031
8	1	6	10	3	0	2	1	23	0.038

9	2	5	5	6	2	2	1	23	0.038
10	6	8	14	3	1	5	1	38	0.062
11	22	14	39	29	8	5	6	123	0.200
12	8398	8593	8513	8576	8588	8473	8718	59859	97.541
total	8760	8784	8760	8760	8760	8784	8760	61368	100

Table 6: Number of NIMROD 1km 5 minute resolution files present within each hour time step between 00:00 01/01/2015 and 23:55 31/12/2021. Total counts for each file number across the full timespan are recorded along with the percentage of the total number of hours observed across the full timespan.

Table 6 shows that over 98% of the individual hours modelled by NIMROD 1km radar have at least one measurement present, with over 97.5% having 12 x 5 minute increments present. In this analysis only hours where all 5 minute files were present for each hour were considered, any hours where one file was missing was discarded.

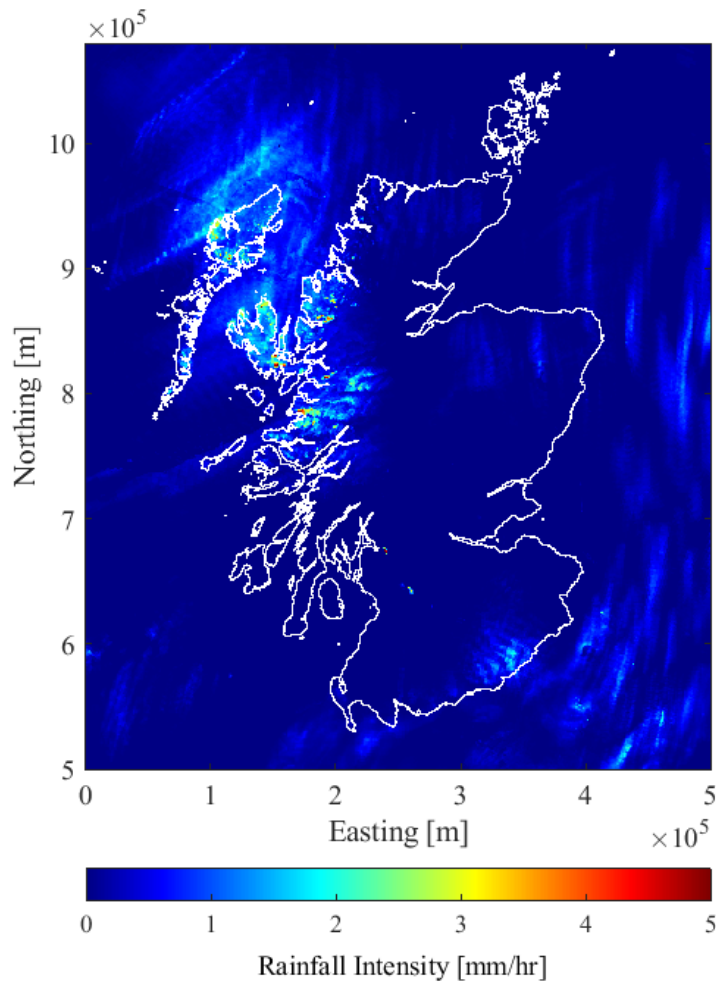


Figure 5: NIMROD 1km radar for Scotland at 01/01/2015 averaged between 00:00 and 00:55.

3.3. Kriging Comparison

A number of different Kriging approaches were tested and the results compared to evaluate which method is most appropriate for the interpolation purposes. The methodology was evaluated at six locations where SEPA stations were located: Newton of Falkland, Esslemont House, Laxdale, Drummore of Cantray, Townfoot and Tobermory. These locations were selected based on their varying proximities to other SEPA stations and NIMROD radar locations listed in Table 7. The reason for doing so was to provide insight into how the accuracy of the kriging process changes with respect to the sparsity of SEPA rainfall stations and radar accuracy. All kriging processes were carried out using the gstools Python package (Müller, et al. 2022).

Test Location Information

Name	Newton of Falkland	Esslemont House	Laxdale	Drummore of Cantray	Townfoot (Glencaple)	Tobermory
StationID	36936	35536	37870	38006	37616	35936
Latitude [Deg]	56.2543	57.3651	57.8687	57.4833	54.9947	56.6203
Longitude [Deg]	-3.1863	-2.1124	-6.8936	-4.0062	-3.569	-6.0806
Easting [m]	326510.7	393241.8	109867.5	279735.2	299634.6	149698
Northing [m]	707491.1	830497.6	897041.6	845418.2	567817.5	755031.5
Altitude [m]	170.6	0	287.2	385.6	45.4	0
Closest SEPA [km]	5.1	13.4	34.3	5.2	14.0	32.5
Closest SEPA Name	Rossie Farm	Balmedie STW	Birkie Hue	Culloden Battlefield	Kinmount House	Polloch
Closest NIMROD [km]	8.8	8.7	56.8	118.4	121.1	133.3

Table 7: Name and proximity information to nearest rain gauge station of test locations.

A total of 6 different kriging applications were performed with the test locations omitted from the dataset: ordinary kriging of SEPA point data with latitude and longitude (OK_{LL}), universal kriging of SEPA point data with latitude and longitude (UK_{LL}), universal kriging of SEPA point data with latitude, longitude and radar (UK_{LLR}), kriging of SEPA point data with altitude as an external drift variable (KED_A), kriging of SEPA point data with latitude, longitude and radar as external drift variables

(KED_{LLR}), and regression kriging of SEPA point data with latitude, longitude and radar as regression variables (RK_{LLR}) The different kriging flavours are described in Appendix A.1.2-A.1.6. The test locations were simulated for the year 2021. Two metrics were used to assess the quality of each kriging process: mean absolute error (MAE) and correlation coefficient (CC). The MAE (Equation 2) gives the average magnitude of errors contained in a set of estimations.

$$\text{Equation 2} \quad MAE = \frac{\sum_{i=1}^n |y_i - x_i|}{n}$$

where y_i is the i -th prediction of observation x_i and n is the total number of observations.

CC (Equation 3) gives the strength of linearity between two variables. It spans between -1 and +1 with -1 indicating perfect negative linearity and +1 indicating perfect positive linearity.

$$\text{Equation 3} \quad CC = \frac{COV(x,y)}{\sigma_x \sigma_y}$$

where $cov(x,y)$ is the covariance of x and y , σ_x is the standard deviation of x and σ_y is the standard deviation of y . Covariance is a measure of the joint variability of two random variables. It quantifies how much two variables change together, or the extent to which they are related to each other. The covariance of variables x and y with length n is given as:

$$\text{Equation 4} \quad cov(x,y) = \frac{\sum_{i=1}^N (x_i - \bar{x})(y_i - \bar{y})}{n-1}$$

where \bar{x} and \bar{y} are the mean values of x and y respectively. If the covariance is positive then the two variable increase or decrease at the same time, if the covariance is negative then they tend to increase or decrease in the opposite direction from one another.

Station Name	Distance to Nearest SEPA station [km]	Distance to Nearest NIMROD station [km]	Kriging Type											
			Ordinary (Lat, Lon) <i>OK_{LL}</i>		Universal (Lat, Lon) <i>UK_{LL}</i>		External Drift (Altitude) <i>KED_A</i>		External Drift (Radar) <i>KED_{LLR}</i>		Regression (Radar) <i>RK_{LLR}</i>		Radar Alone	
			CC	MAE*	CC	MAE*	CC	MAE*	CC	MAE*	CC	MAE *	CC	MAE *
			[mm]		[mm]		[mm]		[mm]		[mm]		[mm]	
Newton of Falkland	5.1	8.8	0.85	0.69	0.85	0.69	0.85	0.69	0.80	<u>0.61</u>	<u>0.88</u>	0.66	0.61	1.76
Esslemont House	13.4	8.7	0.74	0.87	0.76	0.84	0.74	0.88	0.89	0.54	0.89	0.57	0.88	0.64
Laxdale	34.3	56.8	0.38	1.53	0.55	1.34	0.51	1.52	<u>0.72</u>	<u>1.09</u>	<u>0.72</u>	<u>1.09</u>	<u>0.72</u>	1.19
Drummore of Cantray	5.2	118.4	0.77	0.98	0.78	0.96	0.78	0.96	<u>0.81</u>	<u>0.78</u>	0.72	0.93	0.67	1.04
Townfoot (Glencaple)	14.0	121.1	0.79	0.96	0.79	<u>0.92</u>	0.79	0.95	0.78	0.94	<u>0.82</u>	0.99	0.63	1.55
Tobermory	32.5	133.3	0.34	1.62	<u>0.57</u>	<u>1.21</u>	0.49	1.41	0.52	1.28	0.47	1.35	0.33	1.65
mean	-	-	0.65	1.11	0.72	0.99	0.69	1.07	<u>0.75</u>	<u>0.87</u>	<u>0.75</u>	0.93	0.64	1.31

*MAE values were calculated for all observed hourly rainfall values above 1mm.

The mean result across all stations is displayed with the best performing method at each location and overall underlined.

Table 8: Kriging prediction metric results for all test point rainfall locations for 2021.

An interesting result of the kriging methodologies is that different methods work to different degrees for different locations, as shown in Table 8. OK_{LL} is the only model that does not outperform radar estimations alone, indicating kriging’s usefulness in improving rainfall estimations compared with radar and justifies its selection as a methodology. Broadly speaking, inclusion of NIMROD data improved the accuracy of rainfall predictions with the exception of Tobermory for which UK_{LL} performed best. A comparison of Tobermory and Laxdale, which have similar proximities to other point rainfall stations, demonstrates the influence that radar station proximity has on improving hourly rainfall predictions.

As a side point, if new point rainfall stations are to be established, preference should be made for regions where there is not adequate radar cover as this would have the most significant improvement on nationwide rainfall interpolation. Similarly, new radar stations should be deployed for regions that are not well covered by point rainfall stations for the same reason.

Since altitude as an external drift variable did not improve the estimations compared to UK_{LL} for any metric for any location, there have been no further estimations using altitude. While there has been a considerable amount of research into the significance of altitude for rainfall interpolation over longer timespans such as monthly and annual rainfall, this did not seem to be the case for hourly rainfall in this investigation. However, this observation is inconclusive due to the small sample size and short time period of observation. This is an interesting area for future investigation.

KED_{LLR} has the joint highest mean CC across all locations and the best mean MAE across all test locations and thus is selected to estimate the rainfall intensity at the event locations for January 2015 to December 2021. An average CC of 0.75 for KED_{LLR} demonstrates very good correlation between the observed and predicted hourly rainfall.

After processing hourly data, SEPA and Radar intensities have been also aggregated into 3 hour, 6 hour, 12 hour and 24 hour periods with an hour timestep and kriging is carried out on each timestep. Hence 5 datasets were produced, one for each time window with its associated variance estimation.

3.5. Fragility

The approach outlined here provides an estimate of fragility specifically for critical road sections that have experienced at least one disruption during the specified period. The probability of disruption by rainfall of a given intensity $P(D | I=x)$ at a critical location was calculated using Equation 5, dividing the number of failures for a given intensity by the total instances of that intensity across all locations.

$$\text{Equation 5} \quad P(D | I = x) = \frac{\text{number of failures when } I=x}{\text{number of instances when } I=x}$$

To ensure there was a sufficient population of points for the analysis, the intensity measures were divided into bins. For example, the probability of failure due to 10-12 mm of hourly rainfall was determined by dividing the number of failures recorded for that intensity in the IRIS database by the total instances of 10-12 mm rainfall observed at locations where failures occurred. Given that the IRIS database did not contain the time that the event occurred but only the date of the response time, the intensity measures considered were the maximum observed for the intensity measure in the window spanning 24 hours either side of midnight on the event date.

The rainfall Kriging process estimates the intensity associated with each failure and intensities across the recorded length of the database. The process also quantifies the uncertainty in predicting rainfall intensity at unmonitored locations, which increases with distance from monitored ones. This uncertainty was modelled using a Gaussian distribution defined by the mean estimate and standard deviation of the estimate.

To robustly assess conditional probabilities of failure amid this uncertainty, a Monte Carlo technique was incorporated into the methodology. This computational approach involved simulating numerous scenarios by drawing random values from input probability distributions, generated from the process variance of each Kriging model. Conditional probabilities were then calculated using these sampled input values, recording the corresponding outputs. This iterative process generated a comprehensive range of possible outcomes, offering a statistical distribution of results rather than a single deterministic value. The mean and standard deviation (or selected percentiles) of this distribution were used to estimate the probability of different outcomes and assess the overall risk associated with the system.

In this analysis, 100 sample timeseries for each location were generated from the kriging prediction means and standard deviations. The probability theory was then applied to create a normal distribution of probabilities for each intensity, establishing a probability interval using the p-value of 1.96 for 95% confidence.

By utilizing the upper and lower limits of the 95% confidence interval on the y-axis (representing probability) and the bin edges on the x-axis (depicting rainfall intensity), an empirical step plot was constructed, which describes the empirical fragility curve for the given intensity measure. Selecting a specific intensity value along the x-axis allows for the determination of a 95% probability interval, while choosing a probability value along the y-axis provides upper and lower limits of intensity. An example of this type of plot filled with arbitrary intensity units and dummy values is shown in Figure 6.

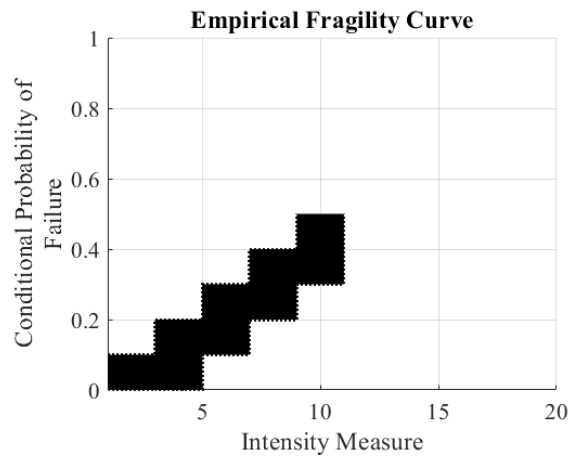


Figure 6: Example empirical fragility curve.

Additionally, a second plot is presented, illustrating the best-fit cumulative distribution function between the upper and lower boundary values. In this process, the highest observed UK value of rainfall for each duration is incorporated as a point, with a corresponding disruption probability of 1. This assumes that if the largest rainfall ever recorded in the UK were to occur on a road section, failure would be inevitable. The UK maximums are recorded in Table 8.

	UK Maximum [mm]
Hourly	92
3 Hour	178
6 Hour	187*
12 Hour	204*
24 Hour	238

Table 9: Met Office UK rainfall records.

*Linearly interpolated value

Using the empirical points and the theoretical maxima, 5 two-parameter cumulative distributions (normal, logistic, lognormal, Weibull and extreme value) were fitted to the points. An example of this for the same dummy values is shown in Figure 7.

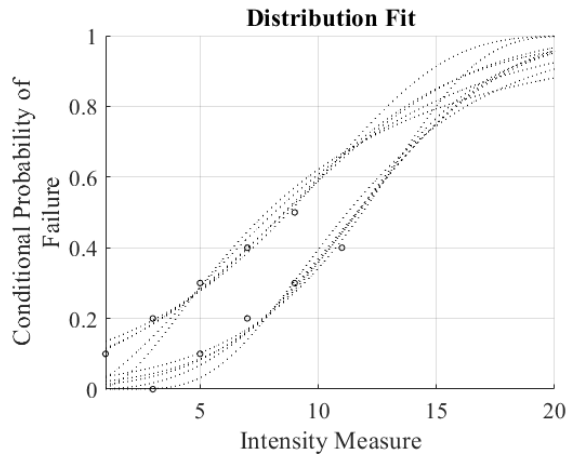


Figure 7: Example distribution fit to dummy empirical conditional probability values.

Finally, a probability box is defined by taking the maximum probabilities of the lower limit and the minimum probabilities of the upper limit. The idea here is that since the shape of the distribution is unknown, a probability box that describes all possible values is presented in order to inform the possible shape of the fragility curve in the unknown region, which can only be truly known through the acquisition of additional data. The probability box associated the dummy values in Figure 7 is shown in Figure 8.

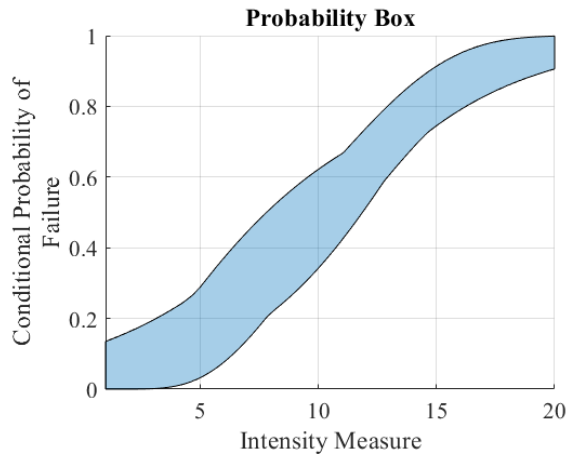


Figure 8: Example probability box for dummy distribution fits.

Since the probability box describes all possible values in the unknown region, application of these curves should be approached cautiously, and it is advised that practitioners use the empirical estimations wherever possible.

4. Results

The results are recorded for peak, 3 hour cumulative, 6 hour cumulative, 12 hour cumulative and 24 hour cumulative rainfall. For the peak rainfall, the peak event in the 24 hours before and the day of the recorded event is selected since the database did not contain a time stamp for the disruption event.

For the cumulative windows, the totals were calculated with a sliding one hour timestep and then the number of events was divided by the size of the window to ensure that all the extreme events were captured, and the results were not distorted by an arbitrary starting position. As with the peak rainfall the largest aggregate rainfall in the 24 hours before and the day of the recorded event was selected.

Each section contains four figures: a histogram showing the distribution of magnitudes associated with each event (including the 95% upper and lower confidence bounds calculated from uncertainty curve based on the distance from the event location to the nearest radar station), an empirical disruption probability curve, the fitting of multiple distributions through the upper and lower estimates and a probability box from the maximum and minimum values associated with the group of distributions.

4.1. 1 Hour (Peak)

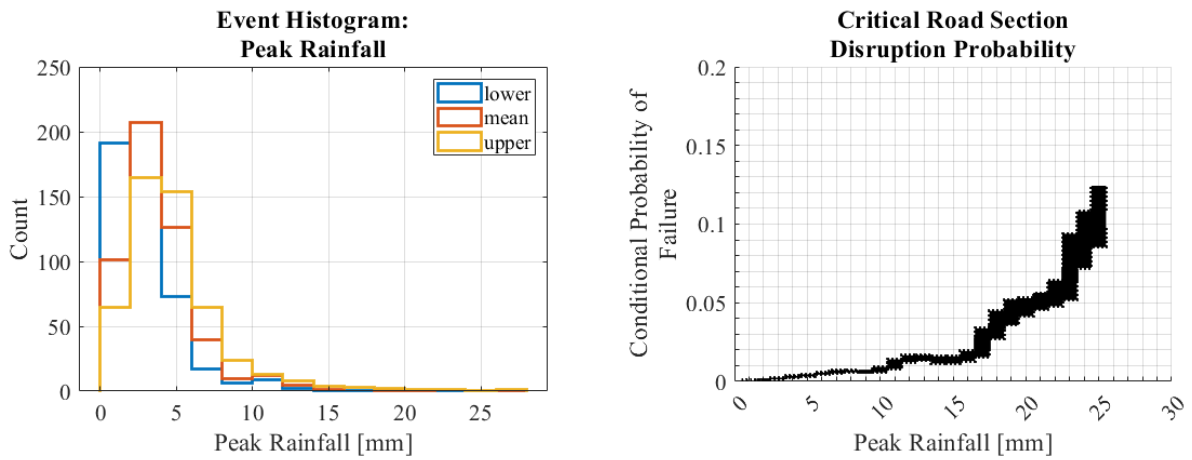


Figure 9: Histogram of mean and lower and upper 95% confidence bounds for peak predictions associated with the 506 disruption events (left). Empirical Disruption/Conditional Probability Curve for Peak Rainfall (right).

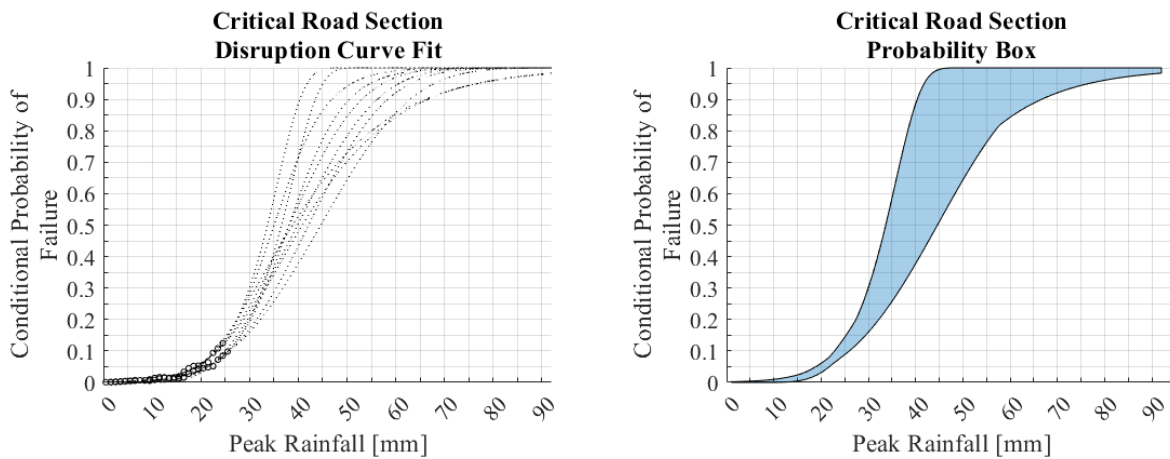


Figure 10: Cumulative distributions fitted to empirical conditional probability values for peak rainfall including UK maximum point (left). Probability box formed by the maximum and minimum values of all fitted distributions.

4.2. 3 Hour Cumulative

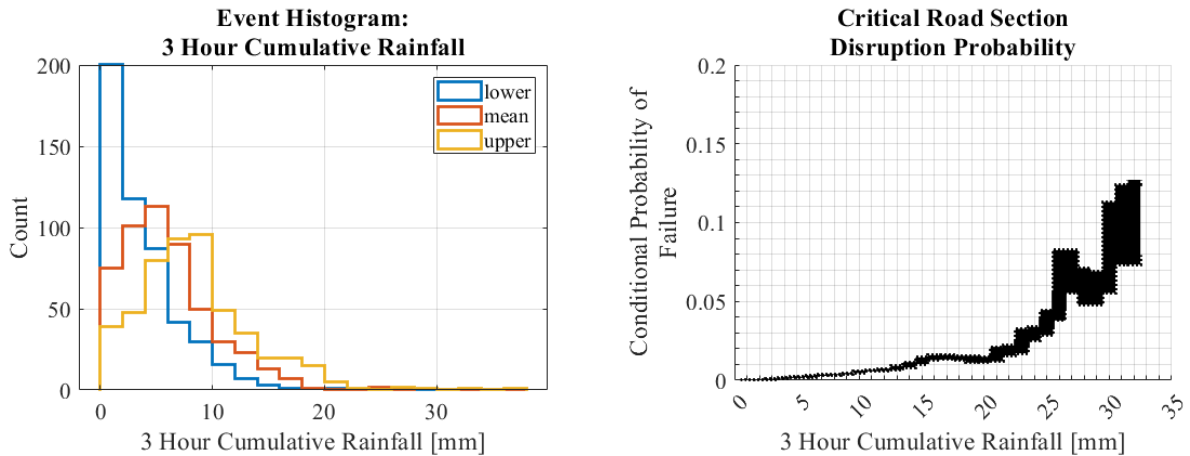


Figure 11: Histogram of mean and lower and upper 95% confidence bounds for 3 hour cumulative predictions associated with the 506 disruption events (left). Empirical Disruption/Conditional Probability Curve for 3 hour cumulative rainfall (right).

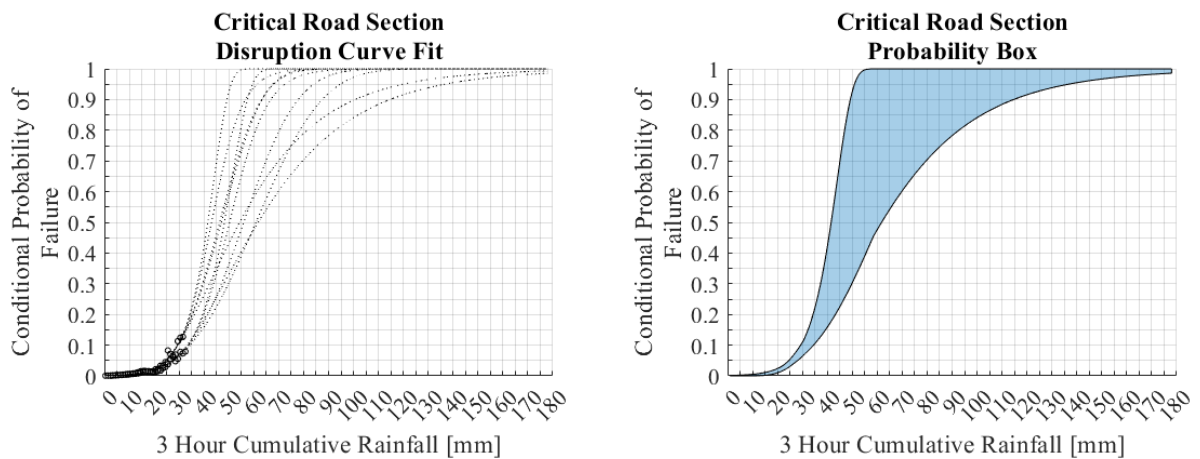


Figure 12: Cumulative distributions fitted to empirical conditional probability values for 3 hour cumulative rainfall including UK maximum point (left). Probability box formed by the maximum and minimum values of all fitted distributions.

4.3. 6 Hour Cumulative

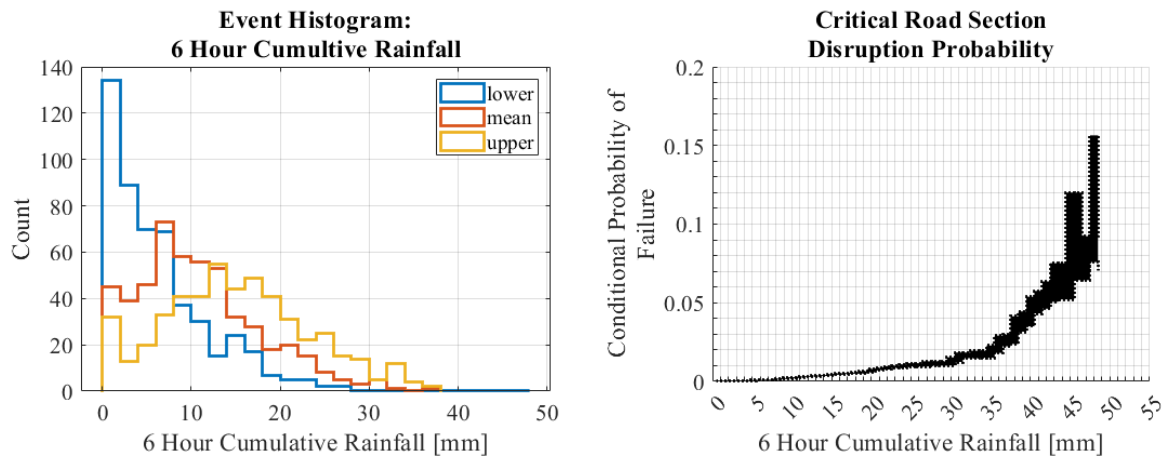


Figure 13: Histogram of mean and lower and upper 95% confidence bounds for 6 hour cumulative predictions associated with the 506 disruption events (left). Empirical Disruption/Conditional Probability Curve for 6 hour cumulative rainfall (right).

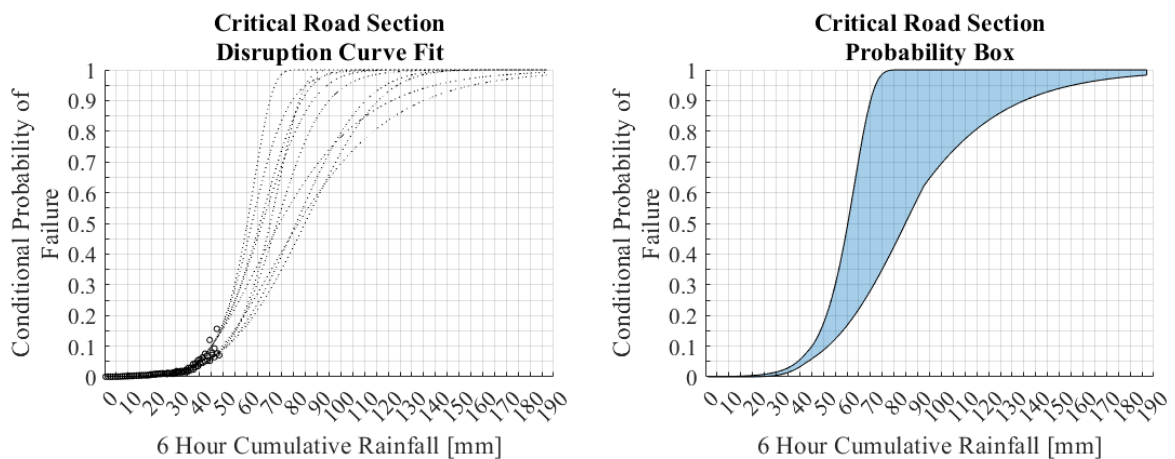


Figure 14: Cumulative distributions fitted to empirical conditional probability values for 6 hour cumulative rainfall including UK maximum point (left). Probability box formed by the maximum and minimum values of all fitted distributions.

4.4. 12 Hour Cumulative

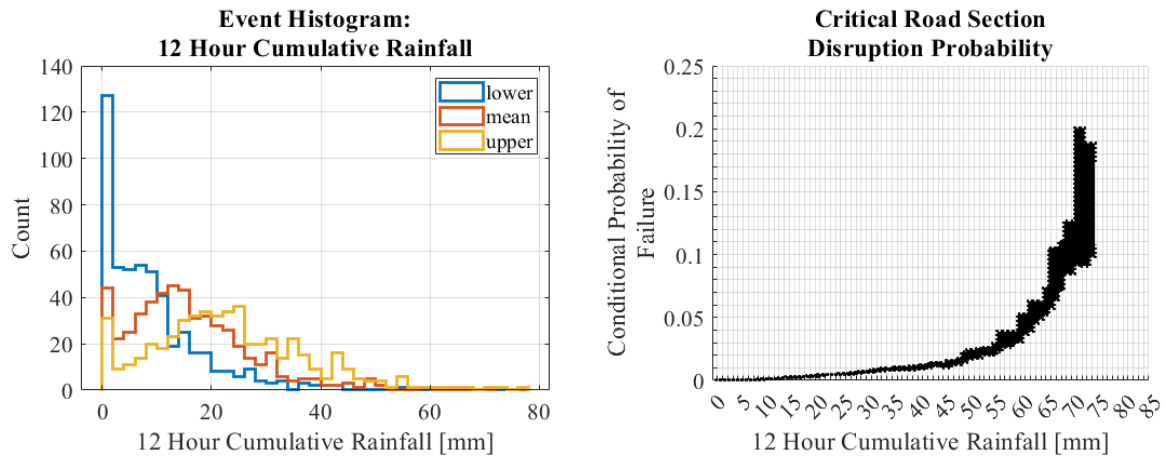


Figure 15: Histogram of mean and lower and upper 95% confidence bounds for 12 hour cumulative predictions associated with the 506 disruption events (left). Empirical Disruption/Conditional Probability Curve for 12 hour cumulative rainfall (right).

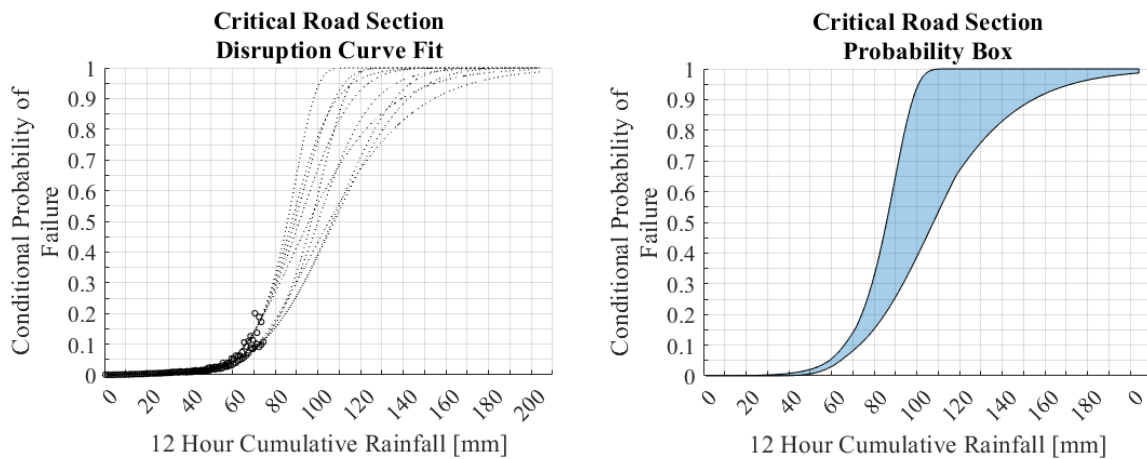


Figure 16: Cumulative distributions fitted to empirical conditional probability values for 12 hour cumulative rainfall including UK maximum point (left). Probability box formed by the maximum and minimum values of all fitted distributions.

4.5. 24 Hour Cumulative

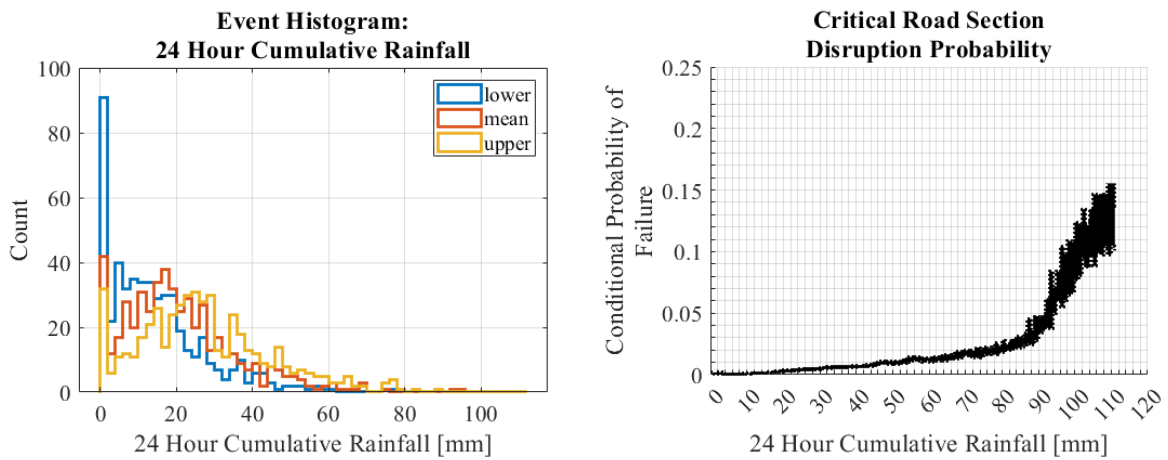


Figure 17: Histogram of mean and lower and upper 95% confidence bounds for 24 hour cumulative predictions associated with the 506 disruption events (left). Empirical Disruption/Conditional Probability Curve for 24 hour cumulative rainfall (right).

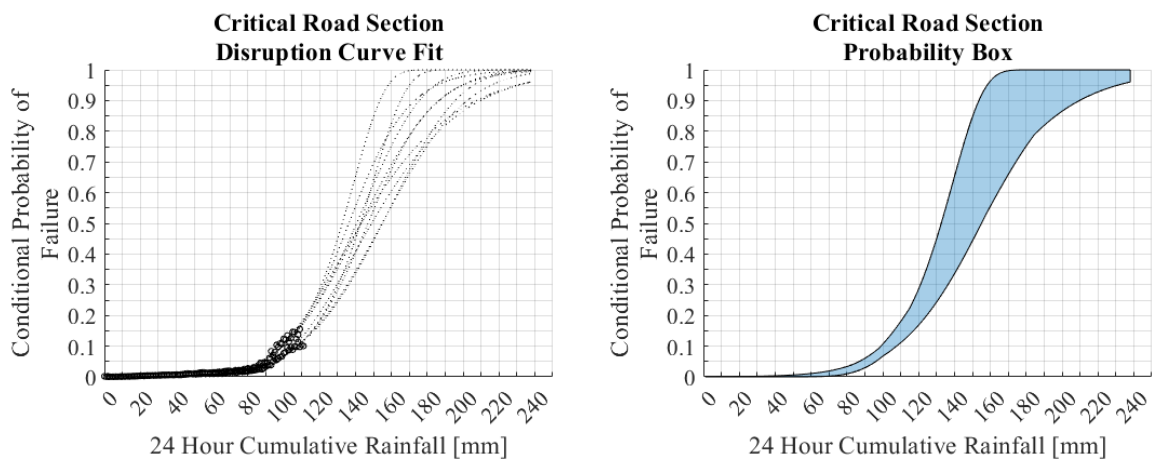


Figure 18: Cumulative distributions fitted to empirical conditional probability values for 24 hour cumulative rainfall including UK maximum point (left). Probability box formed by the maximum and minimum values of all fitted distributions.

5. Conclusion and Discussion

This report has illustrated the methodology developed to build empirical fragility curves for critical road sections belonging to the Scottish Trunk Road network, relating the conditional probability of road failure to the intensity of the rainfall event. Using this methodology, fragility curves have been built by considering different aggregate rainfall observations. The fragility curves are presented with a 95% confidence interval to account for the uncertainty that is present at various stages of the analysis.

While this study fills a critical gap in the quantification of the risk of the Scottish Trunk Road network to extreme precipitation, there are several areas for potential improvement. The analysis is carried out over a 7 year timespan, which may be too short a time period to sufficiently represent the problem or underlying uncertainties. The longer the timespan over which the analysis is considered, the more likely the conditional probability of failure estimates will converge to the true values, and this will also lead to a tightening of the confidence interval. Additionally, the range of rainfall values observed will increase and so the full structure of the fragility curves will become clearer. While distributions have been fitted to the estimated conditional probabilities, it should be noted that extrapolating too far beyond the fitted points is ill advised, and the true structure of the fragility curves in the most extreme regions is unknown. It follows that this process should be repeated when more disruption information data has been gathered.

Furthermore, the analysis is based on the assumption that the IRIS database is representative of the true number of road failures. This is not the case since if multiple failures occur at once, the failures are prioritised by OC's in order of importance and so some road flood events that require attention may go without a response and will not be recorded. Hence the true value of the probability of failure is likely higher than the values that are presented within this report. An adjustment factor based on the response rate of the operating companies could be incorporated into the estimates to make the analysis more robust. Similarly, more precise timing information from the IRIS database would allow for the analysis windows to be tighter and may describe the disruption likelihood more precisely. An investigation into the nature and frequency of simultaneous events would also provide vital vulnerability information but is outside the scope of this investigation. Moreover, in order to estimate the average fragility of the whole network, the developed methodology should be extended by including also the cases of no failure for a given rainfall intensity.

A major area of improvement regards the simplistic approach to the cause of flooding. In essence it is assumed that flood events are caused by rainfall on the road section. This assumption does not take into consideration the relative position of the road to the surrounding landscape or the geometry of the road itself. It is likely that a number of flood events are caused by runoff from the surrounding landscape

and so it may be beneficial to repeat this process using a block or catchment approach where each location is assigned a catchment and the total rainfall for the catchment, perhaps normalized by the area of the catchment, is considered instead of simply the rainfall at each location. This would lead to a more comprehensive understanding of the causes of rainfall related disruption.

Rainfall estimations could be improved through the application of cokriging. At the outset of this investigation, cokriging was ruled out given the increased computational time required to solve the cokriging matrices versus the available computational resource. With additional computing resource, cokriging or co-located cokriging could be applied to give more accurate rainfall estimations. The process variance would likely be smaller and hence the confidence intervals of the fragility curves would be tighter.

As a side note, the analysis considers only the risk of disruption from extreme precipitation. If the overall risk were to be evaluated this analysis would have to be extended to consider risk to life and injury from extreme events through analysis of road accident reports.

References

- Adaption Scotland. 2021. *Climate Projections for Scotland*. Scottish Government.
https://www.adaptationscotland.org.uk/application/files/5716/1114/1258/Climate_projections_for_Scotland_summary_single_page_FINAL.pdf.
- Argyroudis, S, AM Kaynia, S Mitoulis, and M Winter. 2019. "Fragility of transport assets exposed to multiple hazards: State-of-the-art review toward infrastructural resilience." *Reliability Engineering & System Safety*.
- aspexit. 2019. "Introducing the variogram." Accessed 02 20, 2023.
<https://www.aspexit.com/variogram-and-spatial-autocorrelation/>.
- Bertram, A. and Zimmermann, R. 2018. "Theoretical investigations of the new Cokriging method for variable-fidelity surrogate modeling." *Advances in computational mathematics*. Vol. 44. no. 6. pp. 1693–1716.
- Bhattacharjee, Shrutilipi, Soumya Kanti Ghosh, and Jia Chen. 2019. "Semantic Kriging for Spatio-temporal Prediction / [internet resource]."
- Frangopol, D.M. and Kim, S. 2022. "Prognosis and life-cycle assessment based on SHM information." *In Sensor technologies for civil infrastructures*. Woodhead Publishing. pp. 581-607.
- Galasso, C, M Pregolato, and F Parisi. 2021. "A model taxonomy for flood fragility and vulnerability assessment of buildings." *International Journal of Disaster Risk Reduction* 53.
- googleapis. n.d. Accessed Jan 2023.
<https://developers.google.com/maps/documentation/elevation/start>.
- Goovaerts, P. 2000. "Geostatistical approaches for incorporating elevation into the spatial interpolation of rainfall." *Journal of Hydrology*. pp.113-129.
- Harrison, D, S Driscoll, and M Kitchen. 1998. *Improving precipitation estimates from weather radar using quality control and correction techniques*. Forecasting Systems Meterological Office.
- Huizinga, Jan, Hans De Moel, and Wojciech Szewczyk. 2017. *Global flood depth-damage functions: Methodology and the database with guidelines*. Seville: European Comission.
- Mair, A. and Fares, A. 2011. "Comparison of rainfall interpolation methods in a mountainous region of a tropical island." *Journal of Hydrologic Engineering*. p.371.
- Met Office. 2003. "1 km Resolution UK Composite Rainfall Data from the Met Office Nimrod System." NCAS British Atmospheric Data Centre. Accessed March 2023.
<https://catalogue.ceda.ac.uk/uuid/27dd6ffba67f667a18c62de5c3456350>.
- Müller, S, L Schüler, A Zech, and F Heße. 2022. "GSTools v1. 3: a toolbox for geostatistical modelling in Python." *Geoscientific Model Development*. Vol. 15. no. 7. 3161-3182.
- Negreiros, J., Painho, M., Aguilar, F. and Aguilar, M. 2010. "Geographical information systems principles of ordinary kriging interpolator." *Journal of Applied Sciences*. Vol. 10. no. 11. pp.852-867.
- Oliver, Margaret A., and R. Webster. 2015. "Basic Steps in Geostatistics : The Variogram and Kriging." SpringerBriefs in Agriculture. Web.

- Pregolato, M, A Ford, S Wilkinson, and R Dawson. 2017. "The impact of flooding on road transport: A depth-disruption function." *Transport Research- Part D: Transport and Environment*. 67-81.
- Rubinstein, R.Y. and Kroese, D.P. 2017. "Simulation and the Monte Carlo method [internet resource]." *Wiley series in probability and statistics*.
- Salles, M.A., Canziani, P.O. and Compagnucci, R.H. 2001. "Spatial Variations in the Average Rainfall-Altitude Relationship in Great Britain: An Approach using Geographically Weighted Regression." *International Journal of Climatology*. Vol. 21. no. 4. pp.455-466.
- SEPA, Scottish Environmental Protection Agency. n.d. Accessed Jan 2023. <https://www2.sepa.org.uk/rainfall>.
- Stone, D, D Harrison, and R Standing. 2008. *Nimrod System Documentation Paper No.2: Nimrod format for image and model field files*. British Atmospheric Data Centre (BADC). Accessed January 2024. <https://data.ceda.ac.uk/badc/ukmo-nimrod/doc/>.
- Syafrina, A.H., Zalina, M.D. and Juneng, L. 2015. "Historical trend of hourly extreme rainfall in Peninsular Malaysia." Vol. 120. *Theoretical and Applied Climatology*. pp.259-285.
- Transport Scotland. 2014. "Asset Management Systems and Data." Accessed 02 16, 2023. <https://www.transport.gov.scot/publication/road-asset-management-plan-for-scottish-trunk-roads-january-2016/j408891-12/>.
- Transport Scotland. 2014. *The Trunk Road Network, Operating Companies*. Accessed 02 16, 2023. <https://www.transport.gov.scot/transport-network/roads/the-trunk-road-network/#45651>.
- Transport Scotland. 2014. *The Trunk Road Network, Overview*. Accessed 02 16, 2023. <https://www.transport.gov.scot/transport-network/roads/the-trunk-road-network/>.
- Verworn, A. and Haberlandt, U. 2011. "Spatial interpolation of hourly rainfall—effect of additional information, variogram inference and storm properties." *Hydrology and Earth System Sciences*. Vol. 15. no. 2. pp.569-584.
- Vesuviano, Gianni. 2022. *The FEH22 rainfall depthduration-frequency (DDF)*. UK Centre for Ecology and Hydrology.
- Wagner, P.D., Fiener, P., Wilken, F., Kumar, S. and Schneider, K. 2012. "Comparison and evaluation of spatial interpolation schemes for daily rainfall in data scarce regions." *Journal of Hydrology*. pp.388-400.
- Winter, M, B Shearer, D Palmer, D Peeling, C Harmer, and J Sharpe. 2016. "The economic impact of landslides and floods on the road network." *Procedia Engineering*. no. 143. 1425-1434.

Appendix

A.1.1 Expected Value and Semivariance

Before a description of the multiple kriging processes is presented, it is important to introduce the concepts that kriging utilises, mainly expected value, covariance and semivariance.

The expected value of a random variable is the weighted average of the possible values that this function can take (Rubinstein 2017). In the discrete case:

$$\text{Equation 6} \quad E[X] = \sum x p(x)$$

Where $p(x)$ is the probability of x . Another useful quantity is the variance, which measures the spread or dispersion of the distribution from the expected value:

$$\text{Equation 7} \quad \text{Var}(X) = E[(X - E[X])^2]$$

For the normal distribution, the expected value is mean μ and the variance is σ^2 .

Semivariance is used to model the spatial autocorrelation of a random variable or attribute over a geographic region. The semivariance function, also referred to as the experimental variogram, is used to describe the degree of spatial dependence between pairs of observations as a function of distance or lag. In kriging, the semivariance is used to estimate the covariance structure of the underlying random process. The variogram is estimated by applying the Matheron's method, which in one dimension corresponds to the following equation (Oliver 2015):

$$\text{Equation 8} \quad \hat{\gamma}(h) = \frac{1}{2m(h)} \sum_{i=1}^{m(h)} \{z(x_i) - z(x_i + h)\}^2$$

where $\hat{\gamma}(h)$ is the average semivariance between two points at distance h , $z(x_i)$ and $z(x_i + h)$ are the observed values at location x_i and $x_i + h$. When these semivariances are calculated and plotted against their respective lag h , this constitutes the experimental variogram.

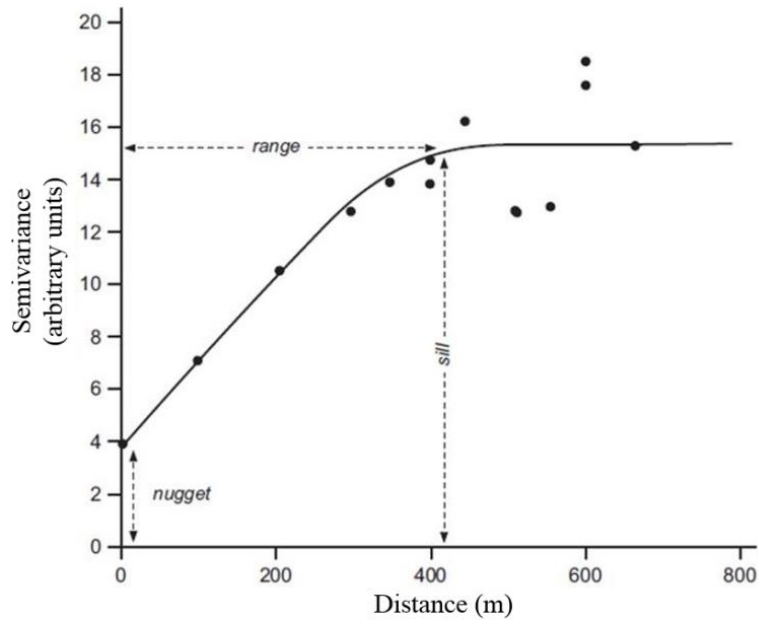


Figure 19: variogram diagram (aspetix 2019).

The variogram in Figure 19 displays three key properties: range, sill, and nugget. The range is the maximum distance at which spatial correlation is present and beyond which it becomes negligible, while the sill is the level of variance observed at this range. The nugget, or non-zero intercept, indicates a discontinuity in variation, which can arise due to measurement errors or variations over distances shorter than the smallest sampling interval. Typically, the nugget variance is a small component of the overall variation (Oliver 2015).

The kriging model's reliability is highly dependent the accurate fitting of the experimental variogram (Oliver 2015). If the variogram describes the variation poorly, then the kriged predictions are also likely to be poor. Accuracy of the variogram depends on the following factors:

- Size of the sample.
- Number of lags used for estimation.
- Lag interval relative to the spatial scale of variation
- Marginal distribution of the variable (probability distribution of the separated behaviour of a single variable in a multivariate system).
- Anisotropy (property where a system exhibits different behaviour in different directions).

For a thorough analysis of the sensitivity of the semivariogram to these factors please refer to Basic Steps in Geostatistics: The Variogram and Kriging, Chapter 3.2 Factors Affecting the Reliability of Experimental Variograms (Oliver 2015).

There are a number of different functions available for fitting the experimental semivariance points, the most common of which are spherical and exponential. Verworn and Haberlandt did an analysis on the spatial interpolation of hourly rainfall and the effect of adding additional information. They stressed the time consuming nature of applying individual variograms to each hourly timestep and suggested generating event specific variograms (Verworn 2011). An alternative is to autofit a number of variograms and select the best performing using a suitable performance metric.

A.1.2. Simple Kriging

In simple kriging the mean of the variable is assumed to be known and constant across the entire study area. The kriging estimator then incorporates this information into the interpolation process. Simple kriging can provide more accurate estimates when the mean of the variable is well-known or easily estimated. In simple kriging, the variance of the estimator depends on the spatial autocorrelation and the estimation error.

Kriging estimates the unknown values at unobserved locations by minimizing the prediction error variance, subject to the constraint that the predictions are unbiased and consistent with the observed values (Oliver 2015). Estimate $\hat{Z}(x_0)$ for unknown location x_0 is calculated by:

$$\text{Equation 9} \quad \hat{Z}(x_0) = \sum_{i=1}^N \lambda_i Z(x_i) + \{1 - \sum_{i=1}^N \lambda_i\} \mu$$

where μ is the constant mean value over the entire region of interest, λ_i are the weights. In simple kriging, the weights assigned to neighbouring data points are determined based on the spatial correlation or covariance structure of the data and are calculated to minimize the estimation error while honouring the assumed mean (Oliver 2015). The simple kriging variance is given by:

$$\text{Equation 10} \quad \sigma_{SK}^2(x_0) = C(0) - \sum_{i=1}^N \lambda_i C(x_i, x_0)$$

where $C(0)$ is the variance of the random process and $C(x_i, x_0)$ is the covariance between known location x_i and target location x_0 (Oliver 2015).

A.1.3. Ordinary Kriging

In real world problems, the true mean and covariance function of the underlying random function $Z(x)$ are unknown, making simple kriging unapplicable for most practical problems. Ordinary kriging does not assume a known constant mean, but assumes a quasi-stationary condition (varying mean but constant covariance) (Negreiros 2010). Ordinary kriging estimates are robust even with moderate departures from stationarity conditions. The mean is assumed stationary in the local search

neighbourhood i.e. a local mean at each point is calculated based on the neighbouring observations. This allows for greater flexibility in modelling the spatial autocorrelation of the variable and can be useful in cases where the mean varies across the study area. In ordinary kriging, the variance of the estimator also includes the estimation error associated with the local mean estimate. Estimate $\hat{Z}(x_0)$ for unknown location x_0 is calculated by:

$$\text{Equation 11} \quad \hat{Z}_{OK}(x_0) = \sum_{i=1}^N \lambda_i Z(x_i)$$

As with simple kriging, the predictions are unbiased. To ensure this the weights of ordinary kriging are constrained to sum to 1 (Oliver 2015):

$$\text{Equation 12} \quad \sum_{i=1}^N \lambda_i = 1$$

The variance of the predictions is given by:

$$\text{Equation 13} \quad \sigma_{OK}^2(x_0) = 2 \sum_{i=1}^N \lambda_i \gamma(x_i - x_0) - \sum_{i=1}^N \sum_{j=1}^N \lambda_i \lambda_j \gamma(x_i - x_j)$$

Where the quantity $\gamma(x_i - x_0)$ is the semivariance of Z between known location x_i and target location x_0 whereas $\gamma(x_i - x_j)$ is the semivariance between the i -th and j -th sampling locations (Oliver 2015).

A.1.4. Universal Kriging

Simple and ordinary kriging assume a stationarity or quasi-stationarity of the real-valued random function $Z(x)$. But in reality the mean value of some spatial data cannot be assumed constant in general, since it will most likely depend on the absolute location of the sample. For example, the intensity of rainfall is higher on average in the west coast of Scotland compared to the east, and spatial variations are observed in the relationship between rainfall and altitude across the UK (Salles 2001). Universal kriging is introduced as a method that splits the random function into a linear combination of non-stationary deterministic functions with a random residual function. The estimation of $\hat{Z}(x_0)$ is the same formulation as before:

$$\text{Equation 14} \quad \hat{Z}(x_0) = \sum_{i=1}^N \lambda_i Z(x_i)$$

where the underlying random function can be expressed as the sum of non-random trend function $\psi(x)$ and residual random function $Y(x)$:

$$\text{Equation 15} \quad Z(x) = \psi(x) + Y(x)$$

Trend function $\psi(x)$ can be evaluated using a regression model. Here the formula is presented for a linear regression model of latitude L_1 and longitude L_2 :

$$\text{Equation 16} \quad \psi(x) = a_0 + a_1 L_1(x) + a_2 L_2(x)$$

Where a_0 , a_1 and a_2 are the regression coefficients. Hence the full estimation term is expressed by substituting Equation 15 and Equation 14 into Equation 11:

$$\text{Equation 17} \quad \hat{Z}(x_0) = \sum_{i=1}^N \lambda_i \{a_0 + a_1 L_1(x) + a_2 L_2(x) + Y(x_i)\}$$

Universal kriging is particularly useful when the trend component of the data is significant and needs to be accurately estimated to make reliable predictions or to perform spatial interpolation as it allows the trend component to be modelled explicitly as a function of the spatial coordinates and estimates both the trend and the residual components simultaneously. Wagner et al. found that for daily rainfall estimates, interpolation methods that use covariates outperform univariate interpolation methods (Wagner 2012).

A.1.5. Kriging with External Drift

If additional variables exist that are linearly related to the target variable, it is possible to incorporate them into the kriging system to improve predictions. In this case the assumption of a constant expected value is replaced with the linear relationship between the target and correlated variable. The formulation of kriging with an external drift is similar to that of universal kriging; however, in the external drift model, the deterministic component (Equation 15) is assumed to be linearly related to a set of auxiliary variables. In the case of kriging with external drift The estimation of $\hat{Z}(x_0)$ is:

$$\text{Equation 18} \quad \hat{Z}(x_0) = \sum_{i=1}^N \lambda_i Z(x_i)$$

For:

$$\text{Equation 19: } \sum_{i=1}^N \lambda_i Z(x_i) \cdot q_k(x_i) = q_k(x_0) \quad \text{for } k=1, \dots, p$$

Where q_k is the k -th predictor variable, p is the number of predictors and the other symbols have their usual meanings. The variance of the predictions is given by:

$$\text{Equation 20} \quad \sigma_{KED}^2(x_0) = C_0 + C_1 - c_0^T \cdot \lambda_0$$

Where C_0 and C_1 are estimated parameters of the semi-variance function, and c_0^T is the extended vector of variances at the new location:

$$\text{Equation 21} \quad c_0^T = \{C(x_0, x_1), \dots, C(x_0, x_n), q_1(x_0), \dots, q_p(x_0)\}^T; \quad q_0(x_0) = 1$$

A.1.6. Regression Kriging

Regression kriging used is alternative to universal kriging but instead of the trend component being modelled explicitly and the trend and residual components simultaneously estimated, the trend component is evaluated using a regression model, such as linear or non-linear regression. Once the regression model is fitted, the residuals of the model, which represent the spatially correlated variation

that cannot be explained by the covariates, are interpolated using ordinary kriging. The trend component and residual estimation are then combined to obtain the final predictions.

Regression kriging has several advantages over traditional kriging methods, including the ability to incorporate covariate information, which can improve the accuracy of the predictions, and the ability to quantify the relative importance of the covariates in predicting the variable of interest.

A.2. Fragility

Fragility is a concept used in reliability engineering to describe the probability of failure of a system or component, given a specific set of conditions or events. It is also known as the conditional failure probability or the conditional probability of non-performance. In reliability engineering, a system or component is considered to have failed if it is unable to perform its intended function or meets some other specified criterion for failure. The probability is a rule that assigns a number between 0 and 1 to a given event, with zero being non chance occurrence and 1 being a certain change of occurrence. The probability of failure is denoted as $P(F)$:

$$\text{Equation 22} \quad P(F) = \frac{N_F}{N_o}$$

Where N_F is the number of failures and N_o is the number of observations. The probability of a rainfall of given intensity x occurring is denoted as $P(I = x)$:

$$\text{Equation 23} \quad P(I = x) = \frac{N_{I=x}}{N_o}$$

Where $N_{I=x}$ is the number of rainfall events with a given intensity x . The conditional probability of failure is calculated by considering the probability of failure given certain conditions. The conditional probability of failure given a certain rainfall intensity level $P(F|I = x)$, is described mathematically as (Rubinstein 2017):

$$\text{Equation 24} \quad P(F|I = x) = \frac{P(F \cap I = x)}{P(I = x)}$$

Where $P(F \cap I = x)$ is the intersection between failure events and rainfall events of a given intensity x :

$$\text{Equation 25} \quad P(F \cap I = x) = \frac{N_{F,I=x}}{N_o}$$

Where $N_{F,I=x}$ is the number of failures when $I = x$. Substituting Equation 25 and Equation 23 into Equation 24 and eliminating N_o yields:

$$\text{Equation 26} \quad P(F|I = x) = \frac{N_{F,I=x}}{N_{I=x}}$$

When this formula is applied to discretised intensity level values, a set of points describing the conditional probability of failure can be produced, Figure 20.

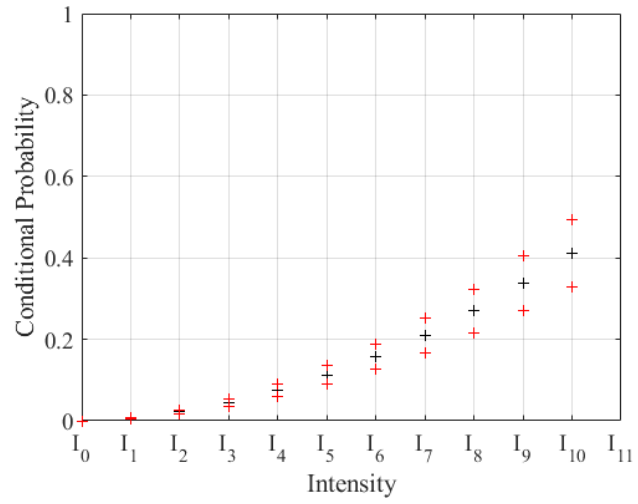


Figure 20: Conditional probabilities for arbitrary intensity measure with regularly spaced intensities showing upper and lower limit of $\pm 20\%$.

A.3. Monte Carlo Method

Monte Carlo methods are a set of computational techniques used to simulate and analyse complex systems or processes. They model the behaviour of a system by extracting random samples from a probability distribution that represents the input parameters of the system being modelled. In the context of this report, each kriging estimation, which is unbiased, has an associated process variance and hence it can be described for each timestep and each location as follows:

$$\text{Equation 27} \quad I_{MC} = E[I] + \varepsilon(0, \sigma_{Krig})$$

Where I_{MC} denotes the intensity of the Monte Carlo sample observation, ε is the error random variable, with Gaussian distribution, zero mean and standard deviation which is the square root of the kriging process variance σ_{Krig} and $E[I]$ is the expected value of the intensity from the kriging estimation.

With the Monte Carlo method, n random samples are drawn from this error distribution for each point and applied to the location and timestep mean prediction. Each Monte Carlo sample is then treated in turn and the conditional probability of failure for the n -th Monte Carlo sample $P(F|I_{MC,n} = x)$ by modifying Equation 21 to:

$$\text{Equation 28} \quad P(F|I_{MC,n} = x) = \frac{N_{F,I_{MC,n}=x}}{N_{I_{MC,n}=x}}$$

With the expected value of the conditional probability for a given intensity over n Monte Carlo samples equal to the mean:

$$\text{Equation 29} \quad E[P(F|I_{MC} = x)] = \frac{1}{n} \sum_{m=1}^n P(F|I_{MC,m} = x)$$

And variance:

$$\text{Equation 30} \quad \text{Var}(P(F|I_{MC} = x)) = E[(P(F|I_{MC} = x) - E[P(F|I_{MC} = x)])^2]$$

By generating a large number of random samples, the Monte Carlo method can provide a comprehensive picture of the possible outcomes of the system. By considering the normal distribution of probability values about the expected conditional probability value, a confidence interval can be defined by 95% z-score with upper and lower bound:

$$\text{Equation 31} \quad \text{upper}_{95\%} = E[P(F|I_{MC} = x)] + 1.96 \sqrt{\frac{\text{var}(P(F|I_{MC} = x))}{n}}$$

$$\text{Equation 32} \quad \text{lower}_{95\%} = E[P(F|I_{MC} = x)] - 1.96 \sqrt{\frac{\text{var}(P(F|I_{MC} = x))}{n}}$$